Investment casting of Ti–46Al–8Nb–1B alloy using moulds with CaO-stabilized zirconia face coat at various mould pre-heat temperatures

Yuan, C.; Cheng, X.; Holt, Grant; Shevchenko, D.; Withey, Paul

DOI:
10.1016/j.ceramint.2014.11.109

Available online at www.sciencedirect.com

ScienceDirect

Ceramics International 41 (2015) 4129–4139

CERAMICS INTERNATIONAL

www.elsevier.com/locate/ceramint

Investment casting of Ti–46Al–8Nb–1B alloy using moulds with CaO-stabilized zirconia face coat at various mould pre-heat temperatures

C. Yuan[a,*], X. Cheng[a], G.S. Holt[a], D. Shevchenko[a], P.A. Withey[a,b]

[a]School of Metallurgy and Materials, The University of Birmingham, Birmingham B15 2TT, England United Kingdom
[b]Rolls-Royce plc, PO Box 31, Derby DE24 8BJ, England, United Kingdom

Received 18 September 2014; received in revised form 14 November 2014; accepted 20 November 2014
Available online 2 December 2014

Abstract

Casting of titanium based alloys presents considerable problems including the extensive interactions that occur between the metal and refractory. An investigation was undertaken to develop a zirconia facecoat suitable to replace current zircon/silica facecoat used in investment casting titanium aluminide alloys. The stability of the zirconia slurry was assessed using pH, viscosity and plate weight, and the mould properties such as friability, strength and permeability were measured. The interaction between the zirconia face coat and a Ti–46Al–8Nb–1B alloy was studied by centrifugal investment casting at three mould pre-heating temperatures. Computer simulation of metal cooling profiles during casting was also carried out to assist the analysis. In this work, a stable zirconia slurry was developed, and the moulds produced using a zirconia facecoat have comparable mechanical properties and better permeability than those made of the traditional zircon/silica facecoat. The friability of the zirconia facecoat was much improved in comparison to that made of yttria face coat. During casting, metal non-fill defects were presented at a low preheat mould temperature of 500 °C. The interaction products found between the metal and mould included a combined $(Ti, Zr)_5(Si, Al)_3$ and $ZrAl_2$ phases, a re-precipitated ZrO_2 phase, and a Al_2O_3 film at the interface. The interaction between mould and metal also caused a high hardness at the interface due to oxygen penetration, which varied with samples using different mould pre-heat temperatures. The suggestion has been made that the mould pre-heat temperature should be less than 1200 °C.

Keywords: D. ZrO_2; Facecoat; Investment casting; Titanium aluminide

1. Introduction

The first attempts to cast titanium alloys were made in 1950 [1] and these alloys are now widely used in the aerospace, energy and chemical industries. Investment casting is a possible manufacturing route to produce near net shape titanium components. The cost of producing titanium components by other fabrication methods is relatively high, as a result of intrinsic raw materials costs and the metal removal cost associated with producing the required shape. Thus, recent attention has focussed on the development of casting alloys containing a large percentage of other alloying elements to reduce reactivity, alloy costs and density. Gamma titanium aluminides are a family of low density, high performance alloys with the potential to replace current Ni-base superalloys used in the production of aero-engine components [2]. Titanium aluminides are difficult to process mainly due to [3]:

- high melting temperature and poor fluidity,
- strong chemical activity of the molten metal,
- low density combined with high viscosity in the molten state.

Extensive interactions occur between the molten alloy and the refractory moulds, leading to a reaction zone with alpha-case on the surface of the casting and oxide inclusions in the bulk alloy. Alpha-case refers to an oxygen-rich interaction layer on the surface of the casting [4], which is detrimental to the mechanical properties

*Corresponding author. Tel.: +44 1214147839; fax: +44 1214147890.
E-mail address: c.yuan@bham.ac.uk (C. Yuan).

http://dx.doi.org/10.1016/j.ceramint.2014.11.109
0272-8842/

of the finished component, and has to be removed by chemical milling or shot blasting.

Traditionally almost all investment moulds use water-based colloidal silica as a binding system [5]. Research has shown [5,6] that the majority of metal–mould interaction is due to reduction of silica, present as binder and filler phases, by both titanium and aluminium in the molten state. In order to further eliminate the interaction between the mould and metal, mould materials with high chemical inertness have been used as the face coat material during the investment casting process. Yttria has been investigated as a mould material with improved chemical inertness during TiAl casting [7], but the limiting factors on the use of this oxide are that yttria sols are exceptionally unstable and prone to gellation and yttria filler is relatively expensive. By considering production costs, face coat materials such as ZrO_2 [8,9] are considered as face coat materials for TiAl alloy casting in industry.

Due to the poor fluidity of gamma TiAl around its melting temperature, the mould for investment casting TiAl is normally pre-heated to help the alloys flow to avoid mis-run and cold laps in the cast parts [10,11]. However, the excessive preheating accelerates metal–mould reaction of titanium castings [12] and may increase the propensity for surface-connected porosity. Therefore, a balance must be found in order to achieve properties according to design requirements. Kim et al. [13] claim that the spiral fluidity of TiAl alloys is directly related to the mould preheating temperature in the range of 400–800 °C. Jovanović et al. [14] showed that defects such as misrun and macropores were found in the casting when the preheat temperature of moulds was below 500 °C. Applying higher preheat temperature between 750 and 800 °C successfully eliminated many of these defects.

In this study, an investigation was undertaken to develop a zirconia facecoat suitable to replace current zircon/silica facecoat in investment casting of titanium aluminide alloys. The stability of the facecoat slurry is assessed by viscosity, pH and plate weight. The properties of the moulds were evaluated by friability, strength and permeability measurement. The interaction between the zirconia face coat and a Ti–46Al–8Nb–1B alloy was studied at a range of preheat temperatures between 500 °C and 1200 °C using full-scale casting. The effect of preheat temperature on reaction was studied with the assistance of simulation of metal cooling profiles during casting at various conditions. The subsequent interaction between mould and alloy was investigated.

2. Experimental procedures

2.1. Slurry development and characterisation

Slurries were mixed from ammonium colloidal zirconia sol (Ti-coat) with a CaO stabilised filler (ABSCO, −325 mesh). The ratio of CaO doped ZrO2 filler to sol was 3.5 kg/l sol. The stability of the resultant slurry was characterised by measurements of viscosity, pH and plate weight. The viscosity was determined from the time required for a definite volume of slurry to flow through the orifice in the bottom of a metal flow cup, in this case 70 ml of slurry passing through a B5 cup with 4.76 mm orifice diameter. To determine the plate weight of slurry, a metal plate with a size of 45 mm × 45 mm was dipped into slurry for 1 min and drained for 150 s. The weight change of the slurry during the initial 150 s was recorded at intervals of 15 s and the reading at 120 s taken as plate weight of slurry.

2.2. Ceramic shell production and characterisation

2.2.1. Mould production

The detailed constituents of the zirconia primary coat and comparable standard zircon/silica primary coat and secondary coats are listed in Table 1. The moulds were made by first investing the wax pattern into the primary slurry. A chosen stucco was then applied by the rainfall sanding method. The coat was dried at a temperature of 21 °C, 50% relative humidity and 0.2 m/s air speed for 24 h. Six backup coats were then applied. An alumino-silicate stucco (IMERYS, Molochite 30/80 mesh) was applied as the secondary stucoo in layers 2 and 3. A coarser alumino-silicate stucco (IMERYS, Molochite 16/30 mesh) was applied as secondary stucoo in layers 4–7. Each secondary coat was dried at a temperature of 21 °C, 50% relative humidity and 3 m/s air speed for 90 min. Finally a seal coat of secondary slurry was applied and dried at a temperature of 21 °C, 50% relative humidity and 3 m/s air speed for 24 h. The wax inside the ceramic mould was then removed by steam autoclaving at 8 bar pressure for 4 min, followed by a controlled de-pressurisation cycle at 1 bar min^{-1} using a Quicklock Boilerclave™ (Leeds and Bradford Boiler Company Ltd., UK).

2.2.2. Friability

The friability test was specifically designed as a quality control procedure to determine the tendency of the solid to be broken into small pieces by friction force. Measuring friability was mainly to assess the degree of sintering and the possibility of incorporating inclusions into the alloys, which could cause a typical contamination occurring in casting. Test samples for friability measurement are produced by shelling wax bars of 20 mm diameter. The samples were weighed, and the internal diameter and the total length of the tubes were also measured. The test brush was pushed through the tube fully, and pulled back through. The samples were reweighed, and the brushed weight subtracted from the initial weight to give change in weight, *G*. The calculation of the

Table 1
Details of shell systems chosen for reaction analysis.

Shell system	Binder	Filler refractory	Stucco refractory
Standard primary	Remet LP colloidal silica	Minco fused silica −200 mesh ECC Molochite −200 mesh	Alumino-silicate 30/80 mesh
Zirconia primary (ZrO_2)	Remet colloidal zirconia	Calcia stabilised zirconia −325 mesh	Calcia stabilised zirconia 50/100 mesh
Standard secondary	Remet LP colloidal silica	Minco fused silica −200 mesh ECC Molochite −200 mesh	Alumino-silicate 30/80 and 16/30 mesh

friability (F) is given by

$$F = \frac{G}{\pi DL} \quad (1)$$

where D is internal diameter, and L is sample length.

2.2.3. Room temperature flat bar strength measurement

Strength measurements were carried out in accordance with BS 1902. Test pieces, approximately 20 mm × 80 mm were cut using a diamond wheel. To simulate casting conditions, bars were heated at 20 °C min^{-1} to the required maximum temperature, 1000 °C in this case, held for 60 min and then furnace cooled to room temperature before testing. Samples were loaded in three-point bending test geometry (primary coat upwards) on an Instron 8500 tensile testing machine. The span length, L, was 50 mm. A load application rate of 1 mm min^{-1} was used. The failure strength, σ_{Max} was calculated as

$$\sigma_{Max} = \frac{3P_{Max}L}{2WH^2} \quad (2)$$

where P_{Max} is the fracture load, and W and H are the width and thickness of sample fracture area respectively.

2.2.4. Permeability measurements

For the measurement of permeability, a test piece former was prepared, consisting of a mullite ceramic tube (6 mm internal diameter and 10 mm outer diameter and 250 mm in length) and a hollow plastic ball (20 mm radius). A hole was cut into the ball and the mullite tube inserted between 5 mm and 20 mm in the ball. A small fillet of wax was used to bond the tube to the ball and act as a sealant. The test pieces were then dipped to produce shell samples. After drying, the samples were heated at 2 °C/min to 700 °C and held for 6 min to burn out the plastic ball. After this, samples were heated at a rate of 20 °C min^{-1} to 1200 °C, held for 60 min and then furnace cooled to room temperature. Testing was carried out in accordance with BS 1902: Section 10.2:1994, at a test temperature of 1200 °C and with a slight adjustment of the equation for the dynamic viscosity of air. The pressure difference and the flow were recorded at 5 and 10 min dwell times. The permeability of the shell, μ (in m^2), was calculated as

$$\mu = \frac{\eta V_c l}{aP} \quad (3)$$

with

$$V_c = \frac{V_1 T}{T_1} \quad (4)$$

where

- η is the dynamic viscosity of air at the temperature of the test (in N s/m^2)
- V_c is the volumetric flowrate of air corrected for expansion at elevated temperatures (in m^3).
- V_1 is the volumetric flowrate of air at room temperatures (in m^3).
- l is the thickness of the shell mould (in m)
- a is the inner surface of the hollow shell mould (in m)
- P is the pressure difference across the test piece (in N/m^2)
- T is the elevated temperature (in Kelvin)
- T_1 is the room temperature (in Kelvin)

2.3. Casting by an Induction Skull Melting (ISM) method

In order to carry out casting and interaction studies, full-scale moulds were produced with zirconia face-coat to assess the interaction during the casting process. The gravity-filled moulds contained 200 mm long bars of 15 mm diameter attached to a conical pouring basin and a wheel-shaped running system. After dewaxing, the moulds were fired at 1000 °C for 1 h, cooled to room temperature and inspected. Moulds were then placed inside a graphite mould heater inside a vacuum chamber containing an Induction Skull Melting (ISM) crucible. The chamber was evacuated to a vacuum of better than 5×10^{-2} mbar and the mould preheated to one of three different temperatures 500 °C, 1000 °C and 1200 °C and soaked for at least 1 h. The vacuum chamber was backfilled with argon to a partial pressure of 200 mbar. A charge of a Ti–46%Al–8%Nb–1%B (at%) alloy was melted in the ISM crucible using a maximum power of 350 kW and poured into the hot mould. The mould heater was turned off and the mould allowed to cool in situ until a temperature of 300 °C was reached. The vacuum chamber was opened to remove the mould which was then cooled to room temperature. Most of the mould material was removed mechanically and the casting lightly shot blasted. Slices from bottom of the cast bars were cut and polished for further analysis. The microhardness profile at the metal–mould interface was obtained using a Mitutoyo MVK-H1 hardness testing machine in order to characterise alpha case penetration; and SEM micrographs with EDX data were taken on a Jeol 7000/Jeol 6060 in order to characterise the metal–mould interface via elemental penetration into the melt.

2.4. Computer simulation of metal cooling profiles

The mould filling and alloy solidification were simulated using the software package ProCAST 10.0. The simulation procedure consisted of the following three steps:

- Mesh generation.
- Model boundary condition and materials properties setup.
- Post processing.

The meshes of the mould and casting were generated with Visual-Mesh 8.5 software. The maximum tetra element size of the casting rods was 0.5 mm; also two boundary layers with a maximum size of 0.1 mm were generated for better simulation of the heat loss to the mould. The mould mesh had a maximum element size of 5 mm. Properties of the TiAl alloy measured by Harding et al. and Cagran et al. [15,16] were used for the simulations. The mould properties were selected from the ProCAST database. The list of the model initial conditions and boundary setup can be seen in Table 2. Post processing on the results was also done with Visual-Mesh 8.5.

3. Results

3.1. Slurry stability study

The pH, viscosity and plate weight variation against mixing time were recorded and are shown in Fig. 1. The viscosity of the slurry increased slightly over time, accompanying the decrease in pH also observed, as shown in Fig. 1a. The change of plate weight showed a similar trend to the change in viscosity, as shown in Fig. 1b. The slurry plate weight change over 150 s is also illustrated in Fig. 2. Initially the slurry dropped off very quickly from the plate but reached a plateau after draining for 70 s.

Table 2
Model initial conditions and boundaries setup.

Initial mould temperature [°C]	500, 1000, 1200
Alloy inlet temperature [kg/s]	1620 °C
Pouring rate	2.5
Alloy mould heat transfer coefficient [W/m^2 K]	2000
Maximum mould filling [%]	98
Maximum time step for filling [s]	0.01

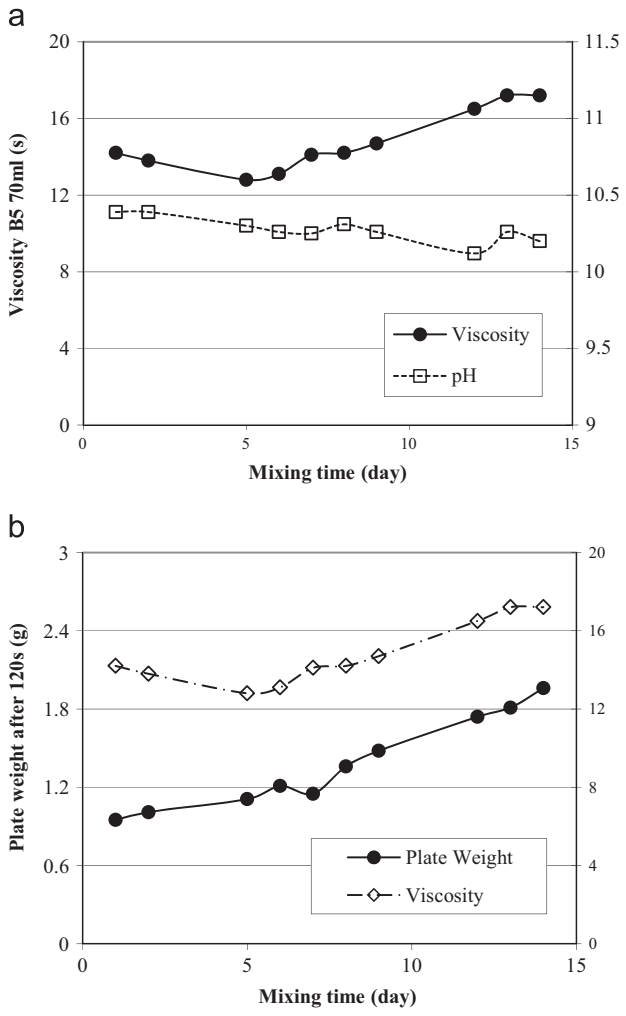

Fig. 1. The properties of zirconia slurry against mixing time: (a) pH and viscosity and (b) plate weight and viscosity.

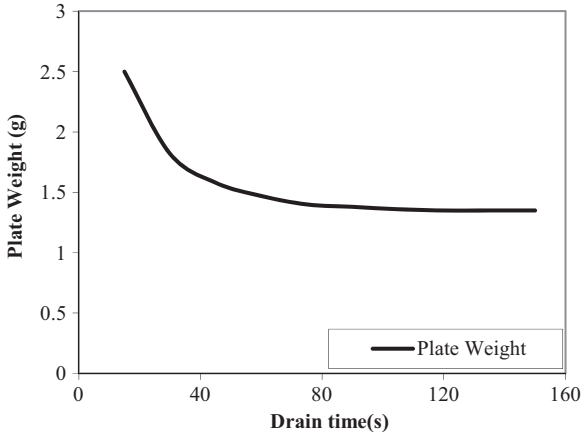

Fig. 2. The draining curve of zirconia slurry over initial 150 s.

3.2. Measurements of the shell properties

The shell thickness, flat bar fracture strength, and permeability results obtained for the shell systems are shown in Table 3. In terms of green and fired strength, the properties of the zirconia shell system were all comparable to that of the standard zircon/silica facecoat shell used for casting steel. The permeability of the zirconia mould is higher in comparison to the standard system. The friability data is illustrated in Fig. 3. For the mould made of zirconia face coat, as sintering temperature increases, friability decreased slightly in a non-linear fashion from 1000 °C up to 1400 °C. This was compared with the friability of the yttria face coat in earlier work [17].

3.3. Metal/mould reaction during casting

3.3.1. Mis-run during casting

To help the alloys flow and to avoid mis-run and cold laps in the cast parts, moulds are pre-heated to three different temperatures: 500 °C, 1000 °C and 1200 °C in this work. When the mould was only pre-heated to 500 °C, the mould was poorly filled by molten metal in the top 80 mm of the bars, as shown in Fig. 4. By increasing the temperature to 1000 °C, the mould was totally filled with only some vein defects found on the surface of metal castings. No filling defects were observed when mould was pre-heated to 1200 °C.

3.3.2. Metal surface examination by XRD

After casting and mould removal, the composition of the metal surface was analysed using XRD, and the results are shown in Fig. 5. It can be seen that very strong ZrO_2 peaks were detected on the metal piece surface in the form of both monoclinic and cubic phase. This is consistent with the facecoat composition. However, SiO_2 peaks were found at the metal surface when cast into moulds pre-heated to 1000 °C and 1200 °C, and the intensities of the peaks increased with increasing mould pre-heating temperature.

Table 3
Comparison of properties of the moulds.

Shell system	Shell thickness (mm)	Green strength (MPa)	Fired strength (MPa)	Permeability ($m^2 \times 10^{-13}$)	
				5 min dwell	10 min dwell
Standard shell	7.54	5.12 ± 0.58	2.85 ± 0.40	5.02	5.26
Shell with zirconia face coat	7.45	5.20 ± 0.70	2.80 ± 0.5	13.33	16.70

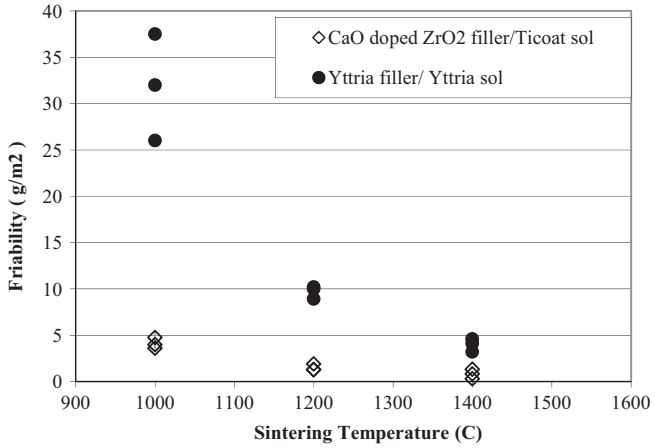

Fig. 3. The comparison of friability of moulds made of CaO doped ZrO_2 facecoat and yttria facecoat [19] at different sintering temperatures.

Fig. 4. The top part of cast bars of different mould pre-heat conditions.

3.3.3. Simulation of metal cooling profiles

The metal cooling temperature profiles of bars with 15 mm diameter at different pre-heat mould temperatures were simulated and are shown in Fig. 6. The fraction of solid at a distance of 150 μm away from the metal surface against solidification time of various bars was modelled and illustrated in Fig. 7. It can be seen that the metal solidification time during cooling is closely dependent on the mould pre-heat temperatures. It takes only 5 s to reach total metal solidification at this point when the mould was pre-heated to 500 °C. When a mould was pre-heated to 1000 °C, it takes 20 s at the same depth to reach total metal solidification. When a mould was pre-heated to 1200 °C, at this depth the time taken to reach total metal solidification increased further to 47 s.

3.3.4. Metal/mould interaction

The microstructure of metal at the metal/shell interface area is shown in Fig. 8. There is a clear $\gamma + \alpha_2$ lamellar structure with the needle like $TiB_{(1,2)}$ phase randomly distributed through the alloy interface. The white particles in Fig. 8(a) are the zirconia fillers from the face coat. The interaction products that were found at the metal/shell interface region are shown in Fig. 8(b)–(e). According to their appearance and locations, they can be generally divided into three different types. Phase A, as shown in Fig. 8b–d, is a light grey phase that appeared mostly at the dendrite boundary, with a certain distance from the interface. Phase B is a bright phase as shown in Fig. 8c, accompanying phase A along the grain boundary. This phase was only found in the sample cast into the mould pre-heated to 1200 °C. Phase C, as shown in Fig. 8e, is a dark phase that mostly appeared at the interface along with the zirconia particles, developing into a thin dark layer at the metal/mould interface, as shown as in Fig. 9. It can be seen that layer thickness was different with different mould pre-heat temperatures. By pre-heating at 500 °C and 1000 °C, the oxidation layer thickness is quite similar at around 1–2 μm, but when the pre-heat temperature was increased to 1200 °C, the oxidation layer thickness increased dramatically to around 15 μm.

The microstructure of the metal cross section was also analysed to determine the penetration distance of the interaction products as shown in Fig. 10, and the results are listed in Table 4. It can be seen that the penetration distance of the interaction products increased with elevated the mould pre-heat temperatures.

3.3.5. Hardened layer

The hardness of metal cast into 500 °C, 1000 °C and 1200 °C preheated moulds was measured from the interface down to 600 μm depth in the metal, and the results are illustrated in Fig. 11. It can be seen that the metal has an average Vickers' hardness value around 350 Hv. All the samples showed high hardness values at the interface region, especially the sample cast in the shell with a pre-heat temperature of 1200 °C. The average hardness of the sample using mould pre-heat set at 1200 °C was above 1150 Hv at the region 10 μm away from interface and for pre-heat at 1000 °C was around 520 Hv, and for pre-heat at 500 °C was 480 Hv. The thickness of the hardened layers were also measured, giving around 100 μm with pre-heat at 500 °C

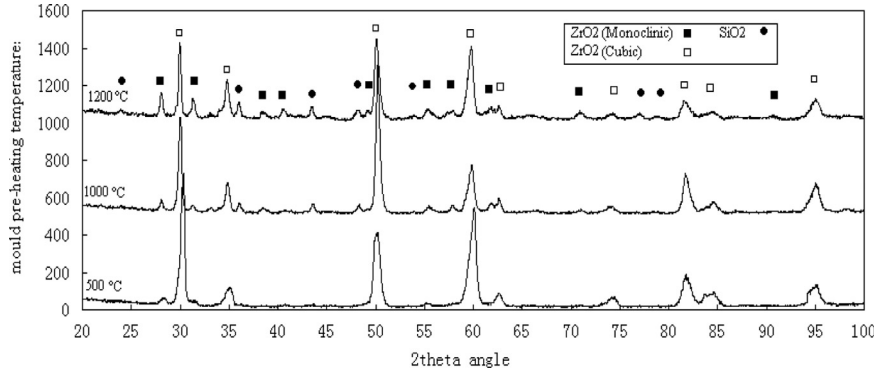

Fig. 5. The XRD test results of the cast metal surface at different mould pre-heat temperatures.

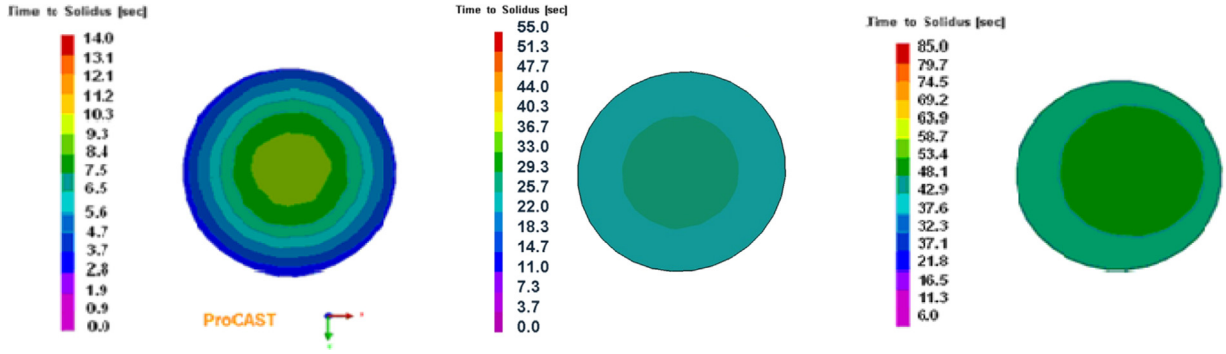

Fig. 6. The simulation of solidification time profile of cylindrical bars of 15 mm diameter during cooling at various preheat temperatures: (a) 500 °C, (b) 1000 °C, and (c) 1200 °C.

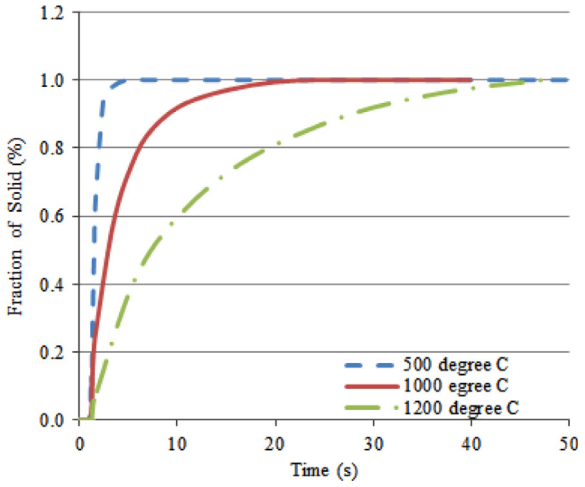

Fig. 7. The fraction of solid against solidification time of 15 mm bars at 150 μm from the surface during cooling at different solidification times.

and 1000 °C temperatures, and around 150 μm at 1200 °C pre-heat temperature.

4. Discussions

4.1. Slurry properties

The increased viscosity, accompanying by the decrease in pH, over time could be related to the evaporation of ammonia and water in the zirconia binder over the mixing time. Those effects can be eliminated by regularly adjusting pH and viscosity with ammonia solution and water, which is a common practice in industry. The slurry is fairly stable over the 15-day period and no gellation effect took place during this period of time. The slurry plate weight change over 150 s shown in Fig. 2 also demonstrates an ideal draining curve for slurry as it provides uniform slurry coating over the wax pattern during the slurry draining period.

4.2. Mould properties

Results shown in Table 3 indicated that, in terms of green and fired strength, the properties of the zirconia shell system were all comparable to that of the standard zircon/silica facecoat shell used for casting steel, so that the mould with the ZrO_2 face coat could withstand the de-waxing and casting processes.

The higher permeability of the zirconia mould in comparison to that of the standard system could be related to microcracks produced due to some degree of zirconia phase transformation which has been previously reported [18]. As the strength of the mould is mainly determined by secondary coats, the decrease in the strength due to microcrack in the primary coat was not observed in this study. Although it is thought that permeability through the shell is less important in vacuum casting, it has been shown that reduced permeability is one of the fundamental factors causing incomplete filling of metal castings [19]. The reduction in gas flow leads to the trapping of residual gases

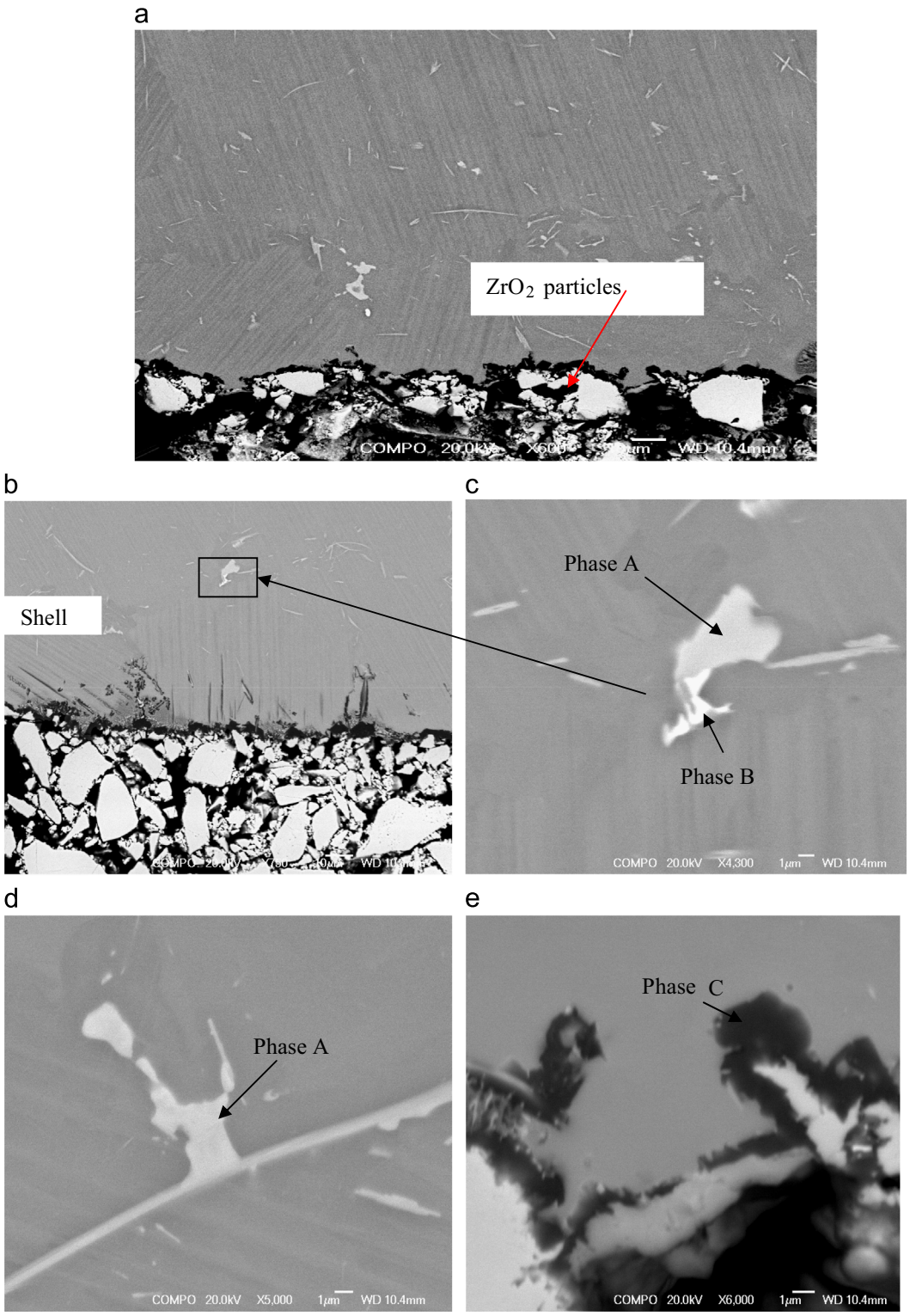

Fig. 8. The microstructure of the TiAl alloy cast into zirconia face-coat mould at 1200 °C pre-heat temperature, showing: (a) the backscatter image of the metal/shell interface region; (b)–(d) location of and morphologies of the phases A and B; (e) location of and morphologies of the dark phase C.

and an increased back-pressure within the cavities of the mould. In turn, this reduces metal flow, especially towards the top of a mould where the metallostatic head is lower. This is especially important for gamma TiAl castings as the alloy density is low and the fluidity is decreased due to the low superheats achieved for these reactive alloys. Therefore the higher permeability in a zirconia mould would be a favourable effect for casting gamma TiAl.

The friability data illustrated in Fig. 3 shows that much better surface sintering properties were found in the zirconia

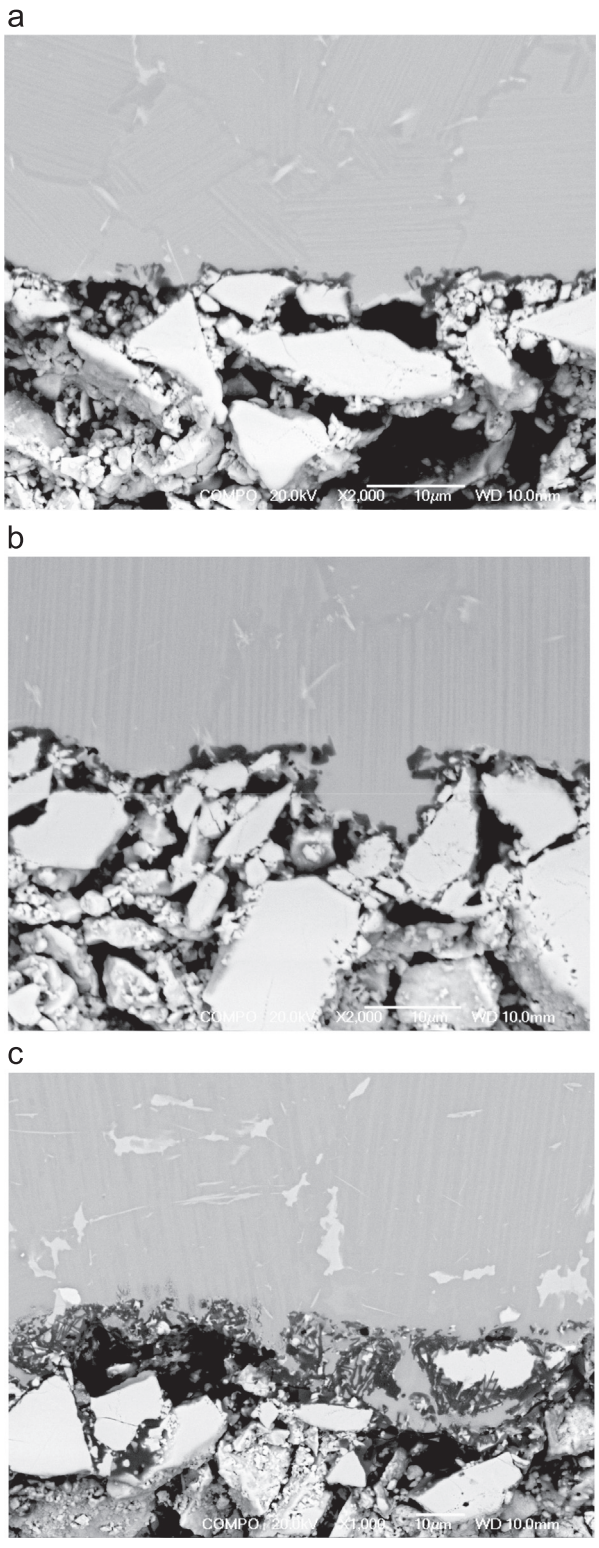

Fig. 9. Microstructure of Ti–46Al–8Nb–1B alloy cast into the moulds with different pre-heat temperatures: (a) 500 °C, (b) 1000 °C, and (c) 1200 °C.

face coat, losing much less solid with friction force. Low friability gives less erosion of the primary coat as metal is poured into the shell, and so reduced inclusion content in the alloy.

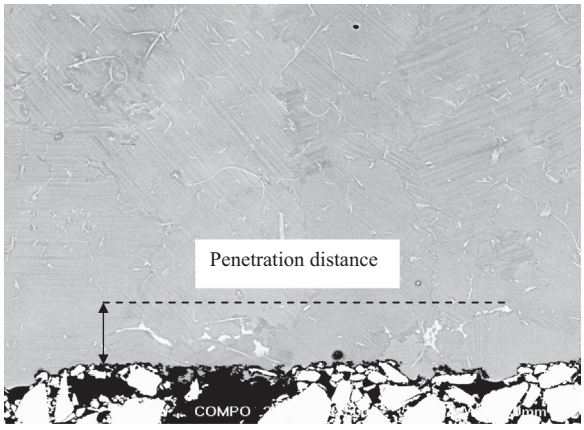

Fig. 10. The backscatter images of microstructures at near metal/shell interface of 15 mm bar cast into mould pre-heating temperatures at 500 °C and the determination of penetration distance.

Table 4
The penetration distance of light phases A and B in metal cast at different mould conditions.

Pre-heat temperatures [°C]	500	1000	1200
Penetration distance [μm]	18.0 ± 6.21	36.4 ± 5.13	57.4 ± 4.37

4.3. Metal/mould reaction

4.3.1. Silicon penetration

Results in Fig. 3 showed SiO_2 peaks were found at the metal surface when cast into moulds pre-heated to 1000 °C and 1200 °C, and the intensities of the peaks increased with increasing mould pre-heating temperature. Because Si was not present in facecoat formulation, as shown in Table 1, the source of the SiO_2 could be traced back to the secondary coats. As the average pore size in the typical primary layers is about 5 μm [17], it is much bigger than the average particle size of SiO_2 particles in sol binder, which is about 0.1 μm in diameter. Similar observations were also made by Yuan et al. [17] and Kim et al. [13] showing the Si penetration effect of TiAl casting using non-silica containing Y_2O_3 and Al_2O_3 face coats.

4.3.2. The interaction between the metal and shell

An EDX analysis revealed that the dendrite boundary phase A was rich in Zr and Si but locally depleted in Ti and Al. The diffraction pattern of this phase shows that it has a complex hexagonal D8 structure, similar to the phase Ti_5Si_3. The study carried out by Chen et al. [20] indicated that Zr has high solubility in TiAl alloy and it is able to dissolve around 11 at% in γ phase, and more than 25 at% in α_2 phase [21,22]. Meanwhile, the study carried out by Kotval and Calder [23] and Cheng et al. [24] indicated that Al ions can dissolve in Ti_5Si_3 to form $Ti_5(Al, Si)_3$ phase. The TEM analysis results in their research found that the phase A was formed of the mixture of two phases $(Ti, Zr)_5(Si, Al)_3$ and $ZrAl_2$.

The bright phase B mainly contains elements Zr and O at an atomic ratio of 1:2, which is confirmed to be ZrO_2. This phase was found by the phase $(Ti, Zr)_2(Al,Si)_3$ region and only

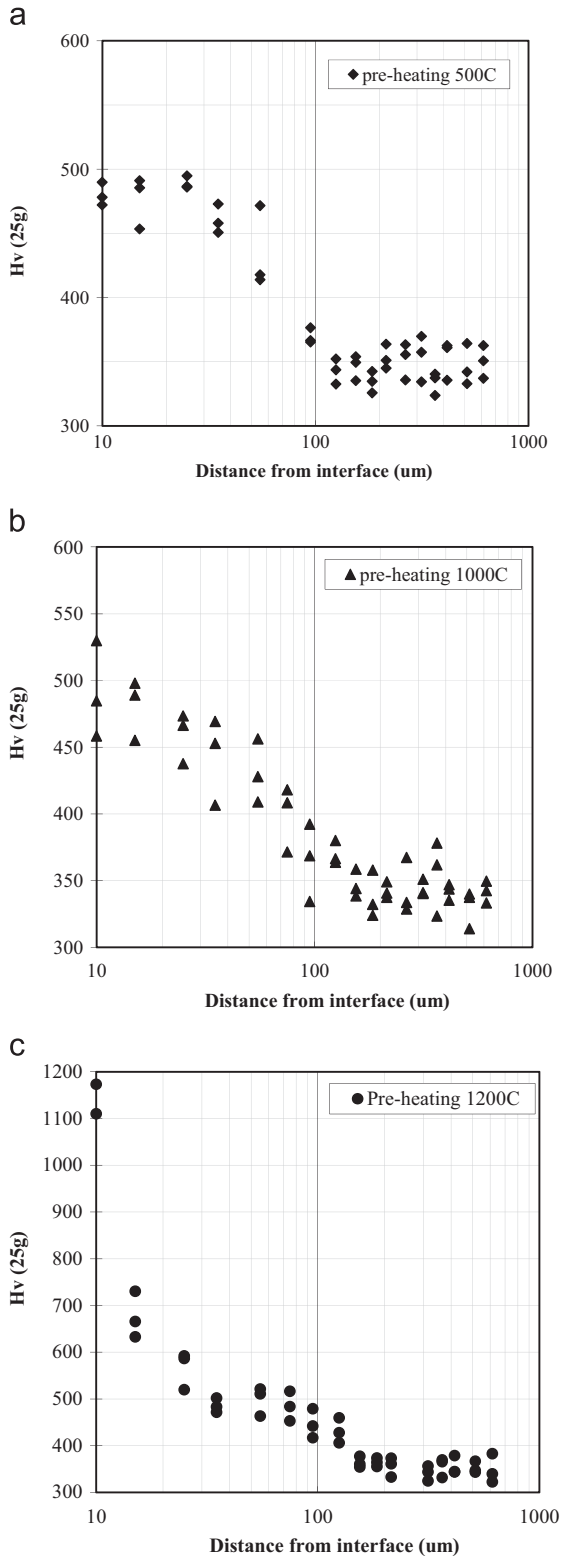

Fig. 11. The hardness of the metal measured from the mould/metal interface to 600 μm depth, for a mould pre-heat temperature of (a) 500 °C, (b) 1000 °C, and (c) 1200 °C.

appeared in the alloy cast in the mould pre-heated to 1200 °C. Previous work [25,26] showed that the zirconia on the mould could be dissolved by liquid metal at high temperature, releasing Zr and O which diffused into the metal. The ZrO_2 dissolution speed becomes much slower when solidification starts. As the solidification time increases with preheat temperature, as described in the previous section, the Zr and O concentration will be higher in the alloy cast in the mould pre-heated to 1200 °C. Due to the negative Gibbs formation energy of ZrO_2, Zr in the $ZrAl_2$ and $(Ti, Zr)_5Si_3$ phase region could be re-precipitated to form the more energetically favourable ZrO_2 when a certain amount of O was diffused into TiAl alloys.

The EDX analysis identified the phase C as Al_2O_3, and it appeared as a continuous film structure forming at the metal/mould interface. This phenomenon was also observed by Barbosa et al. [4] in TiAl alloys interface cast in ZrO_2 mould. According to Ellingham diagrams, when the temperature reaches 750 °C and the solidification has already taken place, Al_2O_3 has higher thermal chemical inertness than ZrO_2, and the chemical reaction between Al in the TiAl and ZrO_2 face coat can be expected as following [27]:

$$2Al_{\text{(in TiAl)}} + 1.5ZrO_2 = Al_2O_3 + 1.5\ Zr_{\text{(in TiAl)}} \quad (5)$$

This reaction leads to the development of a thin oxide layer on metal/mould interface shown in Fig. 9.

4.3.3. *The influence of mould pre-heat temperature*

Simulation of metal cooling profiles shows that a significantly longer time is required for metal to solidify with increasing mould pre-heat temperature, therefore the longer time for the metal and mould interaction and element diffusion. The increased hardness of the metal close to the interfacial region at higher pre-heat casting temperature is likely to be related to the increased oxygen in the same region [28]. Due to the dissolving of ZrO_2 during casting, Zr and O from the face coat were diffused into the metal and the diffusion speed became much slower once solidification began. Therefore the diffusion distance of the oxygen increased with the longer solidification times, resulting in an increased oxygen-hardened layer thickness with elevated mould preheat temperatures. The diffusion distance of elemental O is deeper than the Zr diffusion distance due to the smaller size of the O atom. Therefore the thickness of the hardened layer is larger in comparison to the reaction layer in the metal. A significantly higher hardness value at the surface of the metal cast into the mould pre-heated at 1200 °C was likely to be related to the forming of the Al_2O_3 oxide layer, which increased from 1–2 μm thick at 500 °C and 1000 °C mould preheat temperatures to 15 μm thick at 1200 °C.

5. Conclusion

A mould with ZrO_2 face-coat was successfully developed with stable slurry properties including pH, viscosity and plate weight. The mechanical properties of the zirconia system were comparable with standard zircon/silica based mould system with an improved permeability favourable for liquid metal casting of TiAl. The friability of the zirconia face coat was much improved in comparison with that of yttria face coat used in casting of gamma TiAl.

The effects of the mould pre-heat temperatures on mould filling and surface condition were also studied. Low mould pre-heat temperature of 500 °C results in a non-filled bar, and the metal filling was much improved by increasing mould pre-heat temperature to over 1000 °C. However, a higher mould pre-heat temperature also promoted Si penetration from the backup layer to the face coat, resulting in a reaction within the metal during the casting process. This was coupled with the longer metal solidification time within high preheat mould that accelerated the diffusion of mould material such as Zr, Si and O into the alloy. The computer simulation of metal cooling profiles at various preheat temperatures revealed that, by increasing the mould from 500 °C to 1000 °C and 1200 °C, the metal solidification time of a 15 mm bar increased from 5 s to 20 s to 50 s, which was also confirmed by Zhao, and Oliveira [26,4]. The longer contacting time of molten metals and ceramic shell increased the severity of reaction between metal and ceramic mould.

Microstructural analysis showed that there were three interaction products found in cast metal, which included a grain boundary combined of $(Ti, Zr)_5(Si, Al)_3$ and $ZrAl_2$ phases along with a precipitated ZrO_2 phase at 1200 °C, and Al_2O_3 phase presented as a continuous layer at the metal/mould interface. The depths of the reaction layer increased with preheat temperatures, giving 18.0 μm at 500 °C, 36.4 μm at 1000 °C and 57.4 μm at 1200 °C.

The increased mould pre-heat temperatures also had a significant effect on the hardness value at metal surface which was related to increased oxygen content. The thickness of the hardened layer increased from 100 μm at 500 °C and 1000 °C mould pre-heat temperatures to 150 μm at 1200 °C mould pre-heat temperature. The high surface hardness values corresponded to the thicker Al_2O_3 oxide layer at the higher pre-heat mould temperatures, giving an average of 480 Hv using 500 °C mould pre-heat temperature, 500 Hv using a 1000 °C mould pre-heat temperature and 1150 Hv using a 1200 °C mould pre-heat temperature. The thickness of the Al_2O_3 oxide layer was about 1–2 μm at both 500 °C and 1000 °C, and increased to 15 μm using a 1200 °C mould pre-heat temperature.

The computer simulation of the metal cooling profiles revealed that, by increasing the mould from 500 °C to 1000 °C and 1200 °C, the metal solidification time of a 15 mm bar at 150 μm away from the interface increased from 5 s to 20 s and to 47 s. The longer contact time between the molten metal and ceramic shell increased the severity of the reaction between metal and ceramic mould.

Considering the metal cast properties and the interaction taking place, the paper suggests that the mould pre-heat temperature should be less than 1200 °C.

Acknowledgements

The authors gratefully acknowledge the financial assistance of the UK Engineering and Physical Sciences Research Council (EP/G034907/1) and the support of Rolls-Royce plc for this work.

References

[1] H.B. Bomberger, F.H. Froes, P.H. Morton, Titanium—a historical perspective, Titanium Technology: Present Status and Future Trends, in: F.H. Froes, D. Eylon, N.B. Bomberger (Eds.), Titanium Development Association, Ohio, Dayton, 1985, pp. 3–17.
[2] Y.-W. Kim, H. Clemens, A.H. Rosenberger, in: Gamma Titanium Aluminides, The Minerals, Metals & Materials Society (TMS), USA, ISBN 0-87339-543-3, 2003.
[3] A. Karwinski, J. Stachanczyk, K. Zapalska-Nowak, Titanium casting, Foundry Trade J. 169 (1995) 566–570.
[4] J. Barbosa, H. Puga, C.S. Ribeiro, O.M.N.D. Teodoro, A.C. Monteiro, Characterisation of metal/mould interface on investment casting of c-TiAl, Int. J. Cast Mater. Res. 19 (6) (2006) 331–338.
[5] S. Jones, P.M. Marquis, The role of silica based binders in investment casting, Br. Ceram. Trans. 94 (1995) 68–73.
[6] R.C. Feagin, Casting of reactive metals into ceramic moulds, in: Proceedings of the 6th World Conference on Investment Casting, Washington, USA, 1984, paper 4.
[7] Y. Kobayashi, F. Tsukihashi, Thermodynamics of yttrium and oxygen in molten Ti, Ti_3Al, and TiAl, Metall. Mater. Trans. B 29 (1998) 1037–1042.
[8] Q. Jia, Y.Y. Cui, R. Yang, Intensified interfacial reactions between gamma titanium aluminide and CaO stabilised ZrO_2, Int. J. Cast Met. Res. 17 (2004) 23–28.
[9] K.F. Lin, C.C. Lin, Interfacial reactions between Ti–6Al–4V alloy and zirconia mold during casting, J. Mater. Sci. 34 (1999) 5899–5906.
[10] J. Mi, R.A. Harding, M. Wickins, J. Campbell, Entrained oxide films in TiAl castings, Intermetallics (2003) 377–385.
[11] M.T. Jovanovic, B. Dimicic, I. Bobic, S. Zec, V. Maksimovic, Microstructure and mechanical properties of precision cast TiAl turbocharger wheel, J. Mater. Process. Technol. 167 (2005) 14–21.
[12] M.-G. Kim, Y.-J. Kim, Investigation of interface reaction between TiAl alloys and mold materials, Met. Mater. Int. 8 (2002) 289–293.
[13] M.-G. Kim, S.-Y. Sung, Y.-J. Kim, Microstructure, metal–mold reaction and fluidity of investment cast—TiAl alloys, Mater. Trans. 45 (2004) 536–541.
[14] M.T. Jovanović, I. Bobić, Z. Mišković, S. Zec, Precision Cast Ti-based alloys—microstructure and mechanical properties, J. Metall. 15 (2009) 53–69.
[15] C. Cagran, B. Wilthan, G. Pottlacher, B. Roebuck, M. Wickins, R.A. Harding, Thermophysical properties of a Ti–44%Al–8%Nb–1%B alloy in the solid and molten states, Intermatalics 11 (2003) 1327–1334.
[16] R.A. Harding, R.F. Brooks, G. Pottlacher, J. Brillo, in: Y.W. Kim, H. Clemens, A.H. Rosenberger (Eds.), Gamma Titanium Aluminides, 75, TMS, Warrendale, PA, 2003.
[17] C. Yuan, D. Compton, X. Cheng, N. Green, P.A. Withey, The influence of polymer content and sintering temperature on yttria face-coat moulds for TiAl casting, J. Eur. Ceram. Soc. 32 (2012) 4041–4049.
[18] C. Yuan, P.A. Withey, S. Blackburn, Effect of the incorporation of a zirconia layer upon the physical and mechanical properties of investment casting ceramic shell, Mater. Sci. Technol. 29 (2013) 30–35.
[19] S. Connolly, S. Jones, P.M. Marquis, Mould non-fill in thin walled castings, Foundry Trade J. 172 (1998) 436–440.
[20] X.F. Chen, R.D. Reviere, B.F. Oliver, C.R. Brooks, The site location of Zr atoms dissolved in TiAl, Scr. Metall. Mater. 27 (1992) 45–49.
[21] R. Yang, Y.L. Hao, Y. Song, Z.X. Guo, R. Yang, Y.L. Hao, Z.-X. Guo, Site occupancy of alloying additions in Ti aluminides and its application to phase equilibrium evaluation, Z. Metallkunde 91 (2000) 296–301.
[22] L. Tretyachenko, Al–Ti–Zr (Aluminium–Titanium–Zirconium), in: G. Effenberg, S. Ilyenko (Eds.), Light Metal Systems, Springer, Berlin, Heidelberg, 2006, pp. 1–14 (Part 4).
[23] P.S. Kotval, R.W. Calder, In situ identification of the silicide phase in super-α titanium alloys, Metall. Trans. 3 (1972) 1308–1311.
[24] X. Cheng, X.D. Sun, C. Yuan, N.R. Green, P.A. Withey, An Investigation of a TiAlO based refractory slurry face coat system for the investment casting of Ti–Al alloys, Intermetallics 29 (2012) 61–69.

[25] R.L. Saha, T.K. Nandy, R.D.K. Misra, K.T. Jacob, Evaluation of the reactivity of titanium with mould materials during casting, Bull. Mater. Sci. 12 (1989) 481–493.
[26] R.L. Saha, T.K. Nandy, R.D.K. Misra, K.T. Jacob, On the evaluation of stability of rare earth oxides as face coats for investment casting of titanium, Metall. Mater. Trans. B 21 (1990) 559–566.
[27] R.A. Swalin, in: Thermodynamics of Solids, John Wiley & Sons, USA, 1972.
[28] J. Barbosa, C.S. Ribeiro, A.C. Monteiro, Influence of superheating on casting of γ-TiAl, Intermetallics 15 (2007) 945–955.